Optical Properties of Granular Silver and Gold Films

R. W. Cohen, G. D. Cody, M. D. Coutts, and B. Abeles
RCA Laboratories, Princeton, New Jersey 08540
(Received 22 March 1973)

Optical, electrical, and electron-microscopy studies on granular Ag-SiO_2 and Au-SiO_2 films, prepared by cosputtering the metal and the insulator, were made over the composition range 10–90% by volume SiO_2. Electron diffraction patterns indicate crystalline metals with lattice constants equal to those of the bulk metals. For films with less than 50-vol% SiO_2 the structure consists of amorphous SiO_2 inclusions in a continuous metal matrix; for films with more than 50-vol% SiO_2, separate metallic particles are dispersed in an amorphous SiO_2 continuum. Near the 50-vol% SiO_2 composition the electrical resistivity increases abruptly and the infrared transmission changes from metal-like to insulatorlike behavior. The absorption and transmission peaks in the visible, observed both in the continuous-metal as well as in the continuous-insulator regimes, are explained by a generalized Maxwell-Garnett theory. It is concluded that metal particles as small as 20 Å have optical constants that do not differ significantly from those of the bulk metals.

I. INTRODUCTION

The optical properties of small-metallic-particle systems have been of interest for almost a century. Such systems exhibit a strong characteristic absorption peak which is absent in the bulk metal. For example, in suspensions of gold colloidal particles the absorption peak gives rise to a beautiful ruby-red color. There have been numerous investigations of the optical properties of gold and silver particles[1–6] dispersed in dielectrics or in island film structures. However, no systematic study is available in which the concentration of the metallic phase is varied over the entire range, going from the pure metal to isolated metallic particles. We have undertaken such a study in granular Ag and Au films, which were prepared by cosputtering the metal and SiO_2. We have observed the gradual evolution of the characteristic absorption peaks in the visible and studied the transition from metallic to dielectric behavior in the near infrared.

The previous experimental work was interpreted in terms of the theory of Maxwell-Garnett,[7] which takes into account the modification of the applied electric field at any point within the medium by the dipole fields of the surrounding metal particles. The theory assumes that the metal particles are spherical and small compared to the wavelength of light. In the metal-rich-composition region, where the metal particles coalesce, the Maxwell-Garnett theory breaks down. In order to extend the theory into this composition range, we have treated the metal as a continuum with dielectric inclusions. We have also extended earlier work on the effect of particle shapes in the Maxwell-Garnett theory to include ellipsoidal shapes. The theory is found to be in accord with the present experimental results.

II. EXPERIMENTAL

A. Film Preparation

The granular metal films were prepared by sputtering from composite targets of the metal and the dielectric. The sputtering was rf at 12.56 MHz using argon gas at 4×10^{-3} torr. The self-biased dc cathode voltage was -800 V. The composite targets were made by placing a $\frac{1}{16}$ -in.-thick silica (SiO_2) plate of the appropriate shape on top of a Au or Ag 6-in.-diam disk. The target configurations used for sputtering of the different films and the relative position of the substrate with respect to the target are shown in Table I. The substrates were fused quartz, $\frac{11}{16}$ in. wide, $5\frac{1}{2}$ in. long, and $\frac{1}{16}$ in. thick, and were greased down on a water-cooled substrate holder at a height of $2\frac{1}{4}$ in. above the target. The sputtered film had a continuous variation in composition along its length, being metal rich at the end facing the metallic part of the target and SiO_2 rich in the region facing the part of the target covered by silica. The compositions of the film were determined from the measured thickness of the films using the method of Hanak.[8] This method of composition determination yielded an estimated accuracy of about ±10-vol% SiO_2 in the compositional range 30 to 70-vol% SiO_2. For those compositions outside of this range, the accuracy may be somewhat poorer. Even though the absolute values of the compositions are not known accurately, the relative compositions in a given sputtered strip are known very accurately.[8]

B. Electron Microscopy

The transmission-electron-microscopy studies were made with a Philips EM300 electron microscope with a resolution of about 2 Å. The Ag-SiO_2 and Au-SiO_2 films were sputtered onto carbon films

TABLE I. Target geometry with the indicated dimensions (in inches) used for the different samples. The shaded area indicates metal. The dashed line outlines the position of the substrate above the target.

Sample	Target Geometry
2327, 2407, 2307, 2310	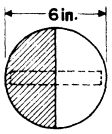
2323, 2316, 2303	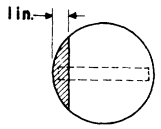
2410	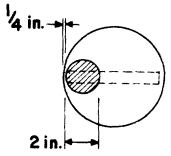

mounted on a copper mesh. The diffraction patterns obtained on the films were characteristic of the constituent metal in the film; the diffraction lines become progressively broader with increasing SiO_2 concentration. The values of the lattice constants were $a_0 = 4.08$ Å for the Ag-SiO_2 films and $a_0 = 4.07$ Å for the Au-SiO_2 films, independent of the SiO_2 concentration up to 80-vol% of SiO_2. These values are close to those of crystalline Ag and Au (4.086 and 4.080 Å, respectively), obtained from x-ray diffraction. The fact that the metal grain lattice constants are close to those of the bulk metal indicates that the SiO_2 does not enter the metal lattice either substitutionally or interstitially. This conclusion is further borne out by the direct observation in the electron micrographs of (111) lattice planes and also by the frequency with which the Moiré fringes occur. The latter observation shows that metal crystallites are superimposed on each other.

The micrographs of the Au-SiO_2 films in Fig. 1 show a matrix inversion from a metal matrix with isolated SiO_2 particles to a SiO_2 matrix with isolated gold particles. In Fig. 1(a) the white circular disks about 20 Å in diameter are probably SiO_2 columns. In Fig. 1(b) the SiO_2 appears as thin curved isolated platelets. Fig. 1(c) shows a labyrinth with a gold continuum and large isolated dendrites of SiO_2. The matrix inversion is complete in Fig. 1(d), which has an SiO_2 continuum with isolated gold particles. It is interesting to note the abruptness of the transition; patterns 1(c) and 1(d) differ by only 10-vol% SiO_2. As the concentration of SiO_2 is further increased, the Au grain size decreases until, for 90-vol% SiO_2, the average size of the Au particles is down to approximately 20 Å. Close inspection of the electron micrographs in Fig. 1 suggests that, in addition to the large Au particles, extremely small Au particles (~ 5 Å) are dispersed in the SiO_2. X-ray line-broadening studies of gold films on quartz gave particle sizes in good agreement to those obtained by electron microscopy, indicating that the sputtered films have very similar structures on the different substrates. Electron microscopy studies on SiO_2-rich Au-SiO_2 cermets by Miller *et al.*[6] show structures similar to those observed in our SiO_2-rich films.

It is possible to estimate the volume percent of the SiO_2 from the electron micrographs. We find that this procedure yields reasonable agreement with the method of Hanak[8] for the SiO_2-rich samples. However, for the metal-rich samples, such as those in Figs. 1(a) and 1(b), the SiO_2 concentrations estimated from the micrographs are appreciably lower than those determined by the Hanak method. The explanation for this discrepancy is not known as yet. In this paper we shall consistently employ the compositions determined by the Hanak method.

Figure 2 shows a similar matrix inversion effect in the Ag-SiO_2 system. However, the labyrinth pattern is not as clear cut as for the Au-SiO_2 films, and some instability of the films was observed in that, with beam exposure, coalescence of the silver crystallites occurred in some samples. Electron micrographs made on Au-SiO_2 and Ag-SiO_2 films of varying thicknesses indicate that the particles are cylindricallike in shape, with the long axis perpendicular to the plane of the film and an average aspect ratio of about 1.7 : 1.

C. Electrical Resistivity

The dc electrical resistivity was measured as a function of composition by evaporating on top of the granular metal gold electrodes, 0.010 in. wide, spaced 0.100 in. along the length of the film. The thicknesses of the films used for the resistivity measurements were about 1 μ. The resistivities measured at 300 °K are plotted as a function of composition in Fig. 3. The abrupt rise in the resistivities near 40-vol% SiO_2 is associated with

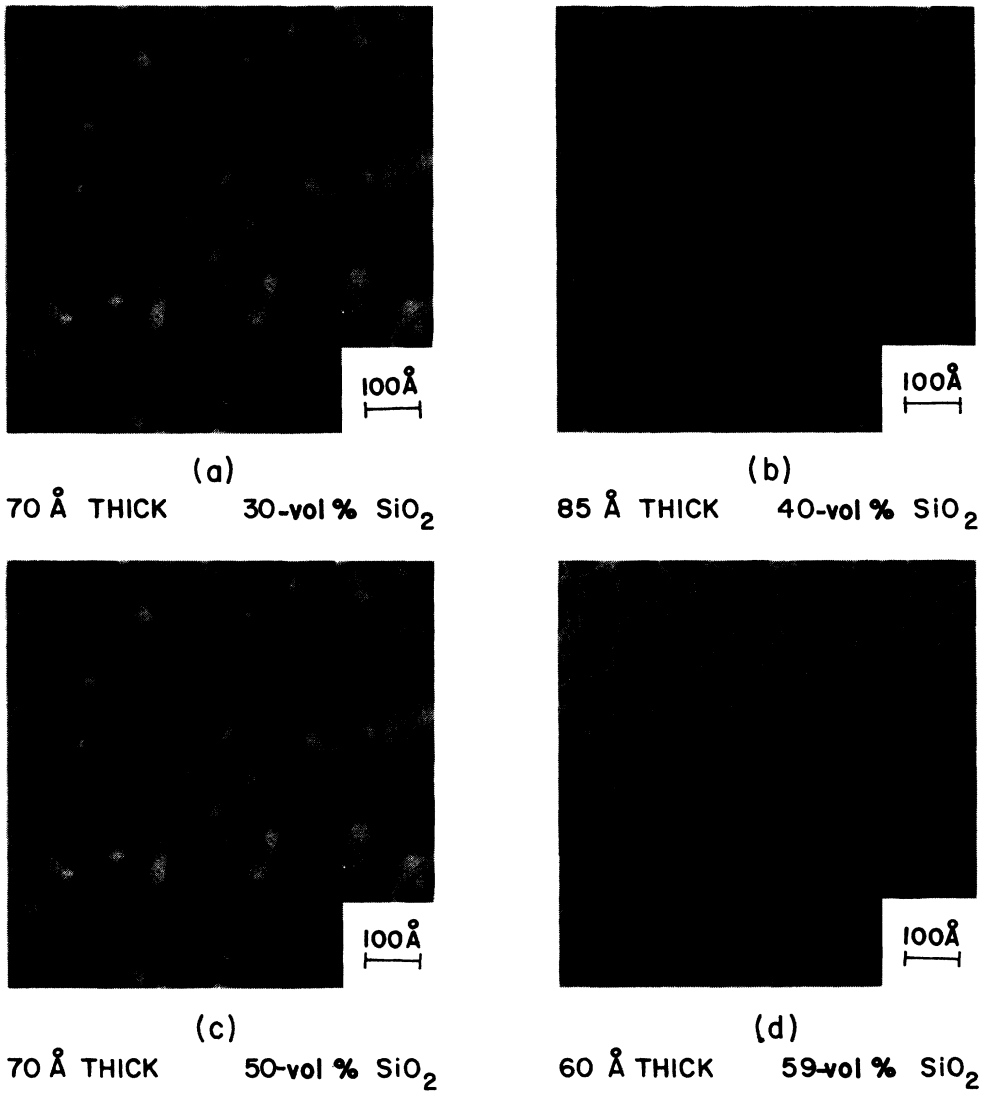

FIG. 1. Electron micrographs of Au-SiO_2 films. Thickness and composition are given in the figure. (a) Au matrix with white circular disks, about 20 Å in diameter, which are probably SiO_2 columns. (b) Au matrix with SiO_2 as thin curved platelets. (c) Au matrix with SiO_2 isolated dendrites. (d) Complete matrix inversion: SiO_2 continuum with isolated Au particles.

the transition of the granular metal from isolated SiO_2 particles in a continuous metal matrix to isolated metal particles in an SiO_2 matrix, as clearly evidenced by the electron micrographs in Figs. 1(c) and 1(d). For films with up to about 50-vol% SiO_2, the resistivity varied only slightly with temperature; for compositions with more than 50-vol% SiO_2, the resistivities increased sharply with decreasing temperature. The above results are in agreement with previous[6,9] work on the electrical properties of granular metals.

D. Optical Measurements

Transmission measurements at normal incidence were made at 300 K on a Cary spectrometer using a rectangular slit 0.2×1.0 cm. The narrow dimension of the slit was parallel to the long direction of the sample. The measured optical densities for several Ag-SiO_2 and Au-SiO_2 films are plotted as a function of wavelength in Figs. 4 and 8. For clarity the curves are displaced vertically with respect to one another. An approximate determination of the relative transmission of the Ag-SiO_2 films can be made using the experimental fact that the optical density at the transmission peak $\lambda_T \cong 3200$ Å was nearly the same for all the Ag-SiO_2 samples. The wavelength λ_A, corresponding to the absorption peak in the visible which

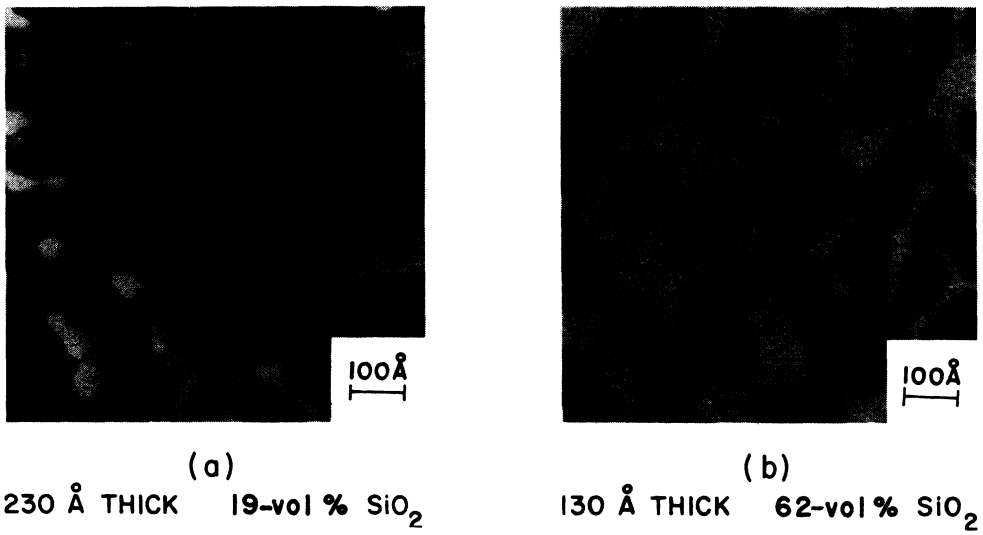

FIG. 2. Electron micrographs of Ag-SiO_2 films. Thickness and composition are indicated in the figure. (a) Ag matrix with white disks which are probably SiO_2 columns. (b) SiO_2 matrix with embedded isolated Ag particles.

develops with increasing SiO_2 concentration, is plotted as a function of SiO_2 concentration in Figs. 5 and 9 for the samples given in Figs. 4 and 8, as well as for the other samples listed in Table I. Also plotted in Figs. 5 and 9 is the wavelength λ_T for which the optical transmission has a relative maximum.

The granular Au films exhibited rotation of the plane of polarization of light when placed between a crossed polarizer and analyzer. This result suggests that the Au particles have a net average orientation in the plane of the film. No such effect was observed for the granular Ag films.

III. THEORY

A. Maxwell-Garnett Theory

The analysis of our experimental results will be based on the dielectric theory of Maxwell-Garnet.[7] This theory takes into account the modification of the applied electric field by the dipole fields of individual polarizable entities, in this case the metal particles. The particles are assumed to be spherical. They must be sufficiently large so that the macroscopic Maxwell equations can be applied to them but not so large that they approach the wavelength (or the attenuation length) of light in the medium. The former condition allows us to characterize the metal particles by a frequency-dependent dielectric constant $\epsilon_m(\omega)$, while the latter condition assures the existence of a dielectric constant $\epsilon(\omega)$ for the ensemble of particles. The size of the Ag- and Au-metal particles encountered

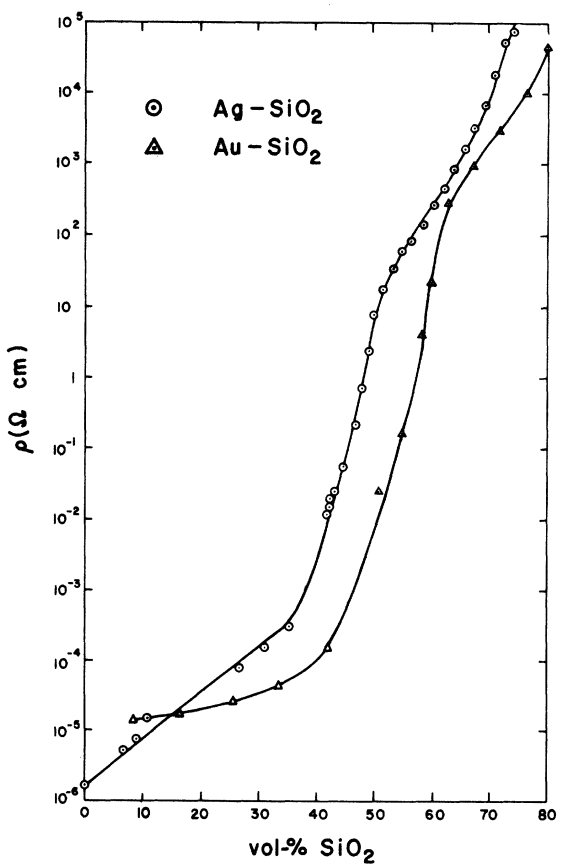

FIG. 3. Electrical resistivities of Ag-SiO_2 and Au-SiO_2 films as a function of volume percent of SiO_2 measured at 300 °K.

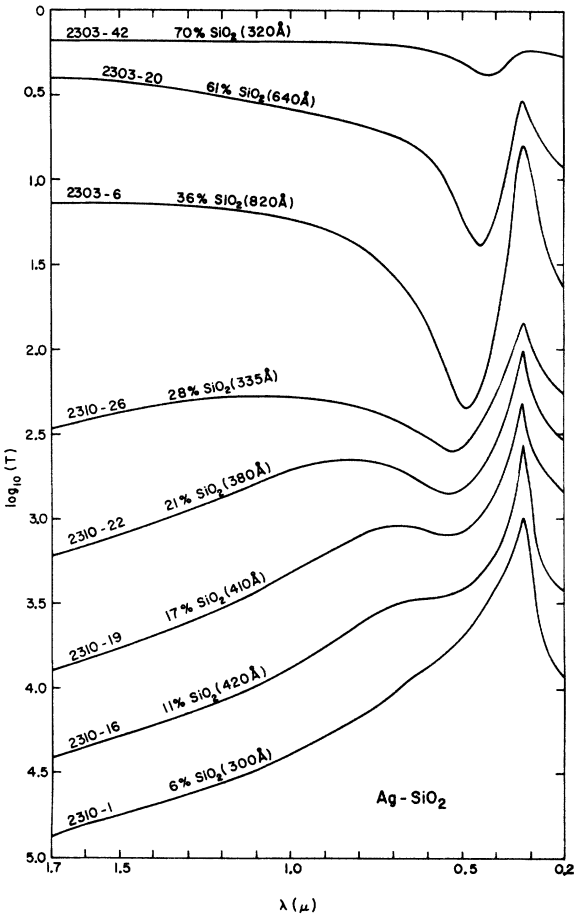

FIG. 4. Logarithms of the optical transmission T of Ag-SiO_2 films, measured at room temperature, as a function of wavelength of light. The sample numbers, the volume percent of SiO_2, and thicknesses are indicated in the figure. The first part of the sample number identifies the particular film strip and target geometry used (see Table I). The second part of the number indicates the distance of the sample (in inches multiplied by 10) measured from the metal-rich end of the strip. For clarity the curves are displaced vertically with respect to one another.

in our experiments appear to meet these criteria.

The derivation of the Maxwell-Garnett result is short and straightforward. One starts with the familiar Clausius-Mosotti equation, applied to a collection of metal particles, which expresses the relationship between $\epsilon(\omega)$ and the volume density n and the polarizability $\alpha(\omega)$ of the metal particles:

$$\frac{\epsilon(\omega)-1}{\epsilon(\omega)+2}=\tfrac{4}{3}\pi n\alpha(\omega)\,. \tag{1}$$

Equation (1) must be modified to take into account the fact that the metal particles are dispersed in a polarizable insulator of dielectric constant $\epsilon_i(\omega)$ rather than in vacuum. Thus, in the calculation of the local electric field, it is necessary to construct a spherical cavity filled with the insulator instead of a completely evacuated cavity, as was the case in the derivation of Eq. (1). We then obtain a generalized Clausius-Mosotti equation:

$$\frac{\epsilon(\omega)-\epsilon_i(\omega)}{\epsilon(\omega)+2\epsilon_i(\omega)}=\frac{4\pi n\alpha(\omega)}{3\epsilon_i(\omega)}\,. \tag{2}$$

Because the metal particles are assumed to be sufficiently large for macroscopic dielectric theory to be applicable, one can substitute for $\alpha(\omega)$ the expression for the polarizability[10] of an isolated metal sphere immersed in a medium of dielectric constant $\epsilon_i(\omega)$. This substitution leads directly to the Maxwell-Garnett result:

$$\frac{\epsilon(\omega)-\epsilon_i(\omega)}{\epsilon(\omega)+2\epsilon_i(\omega)}=(1-x)\,\frac{\epsilon_m(\omega)-\epsilon_i(\omega)}{\epsilon_m(\omega)+2\epsilon_i(\omega)}\,. \tag{3}$$

In Eq. (3), x is the volume fraction of insulator and $\epsilon_m(\omega)$ is the dielectric constant of the metal. The simplicity of this result is self-evident: Given a knowledge of the dielectric constants of the metal and the insulator, and their relative concentration, the dielectric properties of a granular metal can be predicted.

B. Effect of Particle Shape

As was noted above, the Maxwell-Garnett theory assumes the particles to be spherical. In the analysis of our experimental results we shall consider the effect of various particle shapes. Although allowing for nonspherical shapes adds a new parameter to the elegantly simple Maxwell-Garnett theory, it will be of interest to test the sensitivity of the theory, as applied to the granular

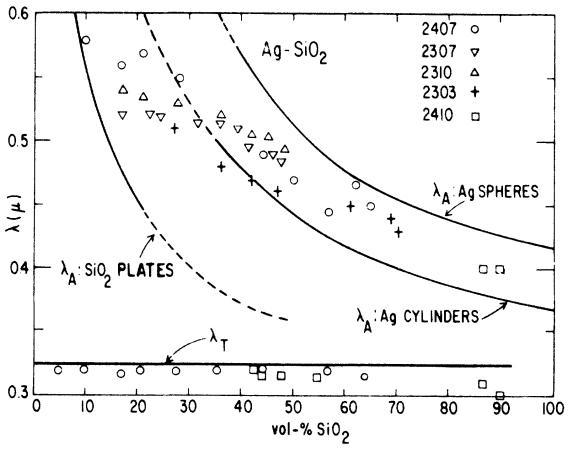

FIG. 5. Absorption-peak wavelength λ_A and the transmission-peak wavelength λ_T as a function of wavelength for several Ag-SiO_2 samples. The curves were calculated from Eqs. (7) and (8) for the particle shapes indicated in the figure. The dielectric constants of SiO_2 ($\epsilon=2.2$) and that of Ag (Ref. 12) were used.

metals, to particle shape.

Galeener,[11] in his treatment of submicroscopic voids in amorphous Ge, has proposed a simple method for treating the case of aligned ellipsoidal particles with the direction of polarization parallel to a principal axis of an ellipsoid. The ellipsoids are assumed to be identical in shape and orientation (but not necessarily in size) with a characteristic depolarization factor L_m. Galeener's result is equivalent to substituting for $\alpha(\omega)$ on the right side of Eq. (2) the expression[10] for the polarizability of an isolated metallic ellipsoid immersed in a dielectric medium. Equation (2) then becomes

$$\frac{\epsilon(\omega)-\epsilon_i(\omega)}{\epsilon(\omega)+2\epsilon_i(\omega)} = \tfrac{1}{3}(1-x)\,\frac{\epsilon_m(\omega)-\epsilon_i(\omega)}{L_m\epsilon_m(\omega)+(1-L_m)\epsilon_i(\omega)}\,. \quad (4)$$

Although, as noted by Galeener, the above equation is valid for x close to unity, inconsistencies arise if one applies Eq. (4) to larger concentrations of metal. For example, for the case $L_m = 0$ (flat metallic plates whose normals are perpendicular to the electric field or long cylinders with axes parallel to the field), we know that there are no induced polarization fields outside an individual particle and, therefore, no modification of the applied electric field. The dielectric constant of the medium should then be the simple weighted average of the individual dielectric constants of the metal and insulator:

$$\epsilon(\omega) = x\epsilon_i(\omega) + (1-x)\epsilon_m(\omega) \text{ for } L_m = 0. \quad (5)$$

However, Eq. (4) does not yield this result except in the limit of small metal concentration. Another case where Eq. (4) leads to an inconsistency is that of flat metallic plates with their normals parallel to the electric field ($L_m = 1$). This case is equivalent to an array of capacitors arranged in series. The correct formula for $\epsilon(\omega)$ is elementary:

$$\epsilon^{-1}(\omega) = x\,\epsilon_i^{-1}(\omega) + (1-x)\,\epsilon_m^{-1}(\omega) \text{ for } L_m = 1. \quad (6)$$

Once again, Eq. (4) does not yield the correct answer for $\epsilon(\omega)$.

The inconsistencies arising from Eq. (4) can be avoided if, in the calculation of the modification of the electric field by the dipole fields of the metal particles, one employs a cavity whose shape is congruent to that of the metal particles; e.g., the cavity is ellipsoidal with depolarization factor L_m associated with the principal axis that is parallel to the electric field. We shall adopt this mathematical construction. The generalized Clausius-Mosotti equation (2) is then modified, and, in place of Eq. (4), we obtain

$$\frac{\epsilon(\omega)-\epsilon_i(\omega)}{L_m\epsilon(\omega)+(1-L_m)\epsilon_i(\omega)} = (1-x)\,\frac{\epsilon_m(\omega)-\epsilon_i(\omega)}{L_m\epsilon_m(\omega)+(1-L_m)\epsilon_i(\omega)}\,. \quad (7)$$

Equation (7) gives the correct results, Eqs. (5) and (6), for $L_m = 0$ and 1, respectively. Naturally, it reduces to the Maxwell-Garnett result, Eq. (3), for the case of metallic spheres $L_m = \frac{1}{3}$. Equation (7) agrees with Eq. (4) in the limit of small metal concentration, giving the same result for $\epsilon(\omega)$ to first order in the quantity $(1-x)$. For larger values of metal concentration, we find that $\epsilon(\omega)$ given by Eq. (7) is less sensitive to departures from sphericity than Eq. (4). To see this, we note that Eq. (7) can be obtained from Eq. (4) by performing the transformation $L_m \to [L_m x + \frac{1}{3}(1-x)]$ in Eq. (4). One can then verify that the variation of L_m over its full range $0 \leq L_m \leq 1$ in Eq. (7) corresponds to a smaller excursion of L_m in Eq. (4).

Since our experiments cover the entire range of x, we shall utilize Eq. (7) to predict the optical behavior of the granular films.

C. Metal-Rich Limit

Although Eq. (7) predicts the correct result $\epsilon(\omega) \to \epsilon_m(\omega)$ in the pure-metal limit $x \to 0$, in practice Eq. (7) is not expected to be valid for small values of x because neighboring metal particles touch and form a labyrinth structure [see Fig. 1 (c)]. Doremus[4] ascribed the failure of the Maxwell-Garnett theory in gold-rich cermets to such an effect. Certainly the physical picture of individual ellipsoidal metal particles breaks down in these circumstances, and it becomes more reasonable to regard the granular metal as consisting of insulating inclusions in a continuous metal matrix, rather than metal particles in a continuous insulating matrix. Such a structure is actually observed in the electron micrographs of Figs. 1(a)–1(c) and 2(a). The appropriate dielectric constant for such a system is obtained simply from Eq. (7) by inverting the role of the metallic and insulating components of the granular metal. We perform the transformations $\epsilon_m \to \epsilon_i$, $\epsilon_i \to \epsilon_m$, $(1-x) \to x$, $L_m \to L_i$ and find

$$\frac{\epsilon(\omega)-\epsilon_m(\omega)}{L_i\epsilon(\omega)+(1-L_i)\epsilon_m(\omega)} = x\,\frac{\epsilon_i(\omega)-\epsilon_m(\omega)}{L_i\epsilon_i(\omega)+(1-L_i)\epsilon_m(\omega)}\,, \quad (8)$$

where L_i is the effective depolarization factor of the insulating inclusions. As we shall see in Sec. III E, Eqs. (7) and (8) display qualitatively different behavior. Thus it should be possible to determine from the optical data the concentration x at which the continuous-insulator picture, described by Eq. (7), goes over into the continuous-metal picture, represented by Eq. (8). As will be shown in Sec. IV, the transition occurs at $x \cong 0.4$.

D. Dielectric Constants $\epsilon_m(\omega)$ and $\epsilon_i(\omega)$

For the metal dielectric constant $\epsilon_m(\omega)$, we have employed the known constants of Ag[12] and Au,[13] modified to take account of the decrease in the conduction-electron relaxation time τ due to the small particle microstructure.[14] Specifically, $\epsilon_m(\omega)$ is decomposed into a free-electron part $\epsilon_m^{(f)}(\omega)$ and an interband part $\epsilon_m^{(i)}(\omega)$:

$$\epsilon_m(\omega)=\epsilon_m^{(f)}(\omega)+\epsilon_m^{(i)}(\omega), \tag{9}$$

where

$$\epsilon_m^{(f)}(\omega)=1+\frac{i\tilde{\omega}_p^2\tau/\omega}{1-i\omega\tau}\ . \tag{10}$$

Here $\tilde{\omega}_p$ is the free-electron plasma frequency. To obtain the values of $\epsilon_m(\omega)$ used in our calculations we have assumed $\epsilon_m^{(i)}(\omega)$ and $\tilde{\omega}_p$ to be unchanged from bulk Ag and Au and have used the value $\tau=2.5\times10^{-15}$ sec, rather than the bulk values $\tau=16\times10^{-15}$ sec for Ag[12] or $\tau=9\times10^{-15}$ sec for Au.[13] For a Fermi velocity of 10^8 cm/sec the small value of τ used here gives rise to a mean free path of 25 Å. According to Doyle,[15] such a mean free path corresponds to a particle size of about 50 Å. Strictly speaking, τ is expected to decrease as the concentration x of the insulating component is increased, falling from the bulk value for particles significantly larger than the bulk mean free path to its lowest value in the insulator-rich regime, where the metal particles reach their smallest size. Evidence for such a size effect is found in the work of Doremus[3] and of Marton and Schlesinger[16] on discontinuous Ni films. In the interest of simplicity we have chosen to neglect the x dependence of τ in our calculations. The effect of the smaller value of τ is primarily to increase the imaginary part of $\epsilon_m(\omega)$ over the bulk value, while leaving the real part relatively little changed. This conclusion follows easily from Eq. (10), once it is realized that, even with the value $\tau=2.5\times10^{-15}$ sec, the quantity $\omega\tau$ is still substantially larger than unity (~3 to 20) in our experiments. Over the wavelength range investigated, the change in the real part of $\epsilon_m^{(f)}(\omega)$ is always less than 8%, while the imaginary part is increased by a factor ranging between 3 and 7, depending on the wavelength and whether Ag or Au is being considered. As will be seen in Sec. III E the wavelength at which observed features occur depends primarily on $\mathrm{Re}\,\epsilon_m(\omega)$; only the magnitude or strength of the features depends on the imaginary part. Thus, uncertainty in the value of τ is not important in understanding the essential aspects of our results.

For the insulator dielectric constant $\epsilon_i(\omega)$, we have used a real, frequency-independent value ϵ_i. Specifically, the value[17] $\epsilon_i=2.2$, characteristic of fused quartz in the visible, was employed in all the calculations. This approximation is expected to be valid if (i) the wavelengths investigated do not coincide with the fundamental SiO_2 absorption bands, and if (ii) the tunneling of electrons from separated metal particles through the insulator, or increased insulator conduction due to possible doping of the insulator by the metal, can be neglected. The first condition is expected to be well satisfied in our experiments, but the second condition requires closer attention. In order for the tunneling contribution to $\epsilon_i(\omega)$ to be negligible we must have

$$\epsilon_i \gg 4\pi\sigma_T/\omega, \tag{11}$$

where σ_T is the effective tunneling conductance of the insulator. We can use Eq. (7) to relate σ_T to the observed dc conductivity $\sigma=(4\pi i)^{-1}\lim_{\omega\to0}[\omega\epsilon(\omega)]$ in the insulator-rich regime. Assuming spherical particles, $L_m=\frac{1}{3}$, and taking $\epsilon_m(\omega)\gg\epsilon_i(\omega)$ (the conductance is limited by the insulator), Eq. (7) gives

$$\sigma=\sigma_T(3-2x)/x. \tag{12}$$

Combining Eq. (12) with the condition (11), the condition on the resistivity $\rho=1/\sigma$ is

$$\rho\gg\frac{4\pi}{\omega\epsilon_i}\,\frac{x}{3-2x}\ . \tag{13}$$

For $x=0.4$ [the smallest value of x for which our experiments show Eq. (7) to be valid] and for the longest wavelength measured, 1.7 μ, the above condition is

$$\rho\gg8\times10^{-4}\ \Omega\ \mathrm{cm}.$$

As can be seen from Fig. 3, the measured resistivities are approximately equal to this value at $x=0.4$ and increase with x far faster than the right side of the condition (13). Thus, we are justified in neglecting the effect of electron tunneling in $\epsilon_i(\omega)$ for $x\gtrsim0.4$. For smaller values of x, Eq. (8) applies, and the conductivity is determined by percolation through long metallic paths, so that σ_T can not be obtained directly from σ. Some experimental evidence will be presented in Sec. IV that the approximation of $\epsilon_i(\omega)$ by a real constant does indeed break down for small values of x.

E. Predictions of the Theory

The important predictions of the theory involve the infrared behavior, the presence of a dielectric anomaly below the plasma frequency, and the plasma frequency itself. We now discuss, in turn, each of these characteristic features.

1. Infrared Behavior

The infrared behavior of granular metals is obtained from Eqs. (7) and (8) by proceeding to the limit[18] $|\epsilon_m(\omega)|\gg|\epsilon_i(\omega)|$. This limit is well obeyed for the dielectric constants of Ag, Au, and SiO_2, for wavelengths larger than about 1 μ. We easily obtain the following formulas for $\epsilon(\omega)$:

$$\epsilon(\omega)=\epsilon_i\left(1+\frac{1-x}{xL_m}\right) \quad \text{(continuous insulator)}, \tag{14a}$$

$$\epsilon(\omega)=\epsilon_m(\omega)\frac{(1-x)(1-L_i)}{1-L_i(1-x)} \quad \text{(continuous metal)}. \tag{14b}$$

From Eq. (14a) it is seen that, in the continuous-insulator regime appropriate for high insulator concentrations, the infrared dielectric constant of the granular metal is determined only by that of the insulator and the values of x and L_m. Therefore, one expects the infrared transmission of a granular metal film to be high and independent of frequency; the granular metal acts as a dielectric. On the other hand, Eq. (14b) predicts that $\epsilon(\omega)$ in the continuous-metal regime is determined by the metal dielectric constant $\epsilon_m(\omega)$, along with the values of x and L_i. Consequently, in this regime the theory predicts that the infrared transmission will be characteristic of that of a metal, i.e., small and increasing with frequency. Thus, the infrared transmission is expected to be a useful tool for investigating the transition from metallike to insulatorlike behavior in granular metals.

2. *Dielectric Anomaly*

Equations (7) and (8) predict the existence of a dielectric anomaly in $\epsilon(\omega)$. An approximate expression for the frequency ω_a at which the anomaly occurs can be obtained from Eqs. (7) and (8) by neglecting $\mathrm{Im}\epsilon_m(\omega)$ and seeking the condition for which $\epsilon(\omega)\to\infty$. This procedure easily yields.

$$\epsilon_m(\omega_a)=-\epsilon_i\left(\frac{1}{L_m x}-1\right) \quad \text{(continuous insulator)} \tag{15a}$$

$$\epsilon_m(\omega_a)=-\frac{\epsilon_i L_i(1-x)}{1-L_i(1-x)} \quad \text{(continuous metal)}. \tag{15b}$$

From Eqs. (15) we see that the anomaly is predicted to occur for negative values of ϵ_m and to shift to larger (less negative) values of ϵ_m as x is increased. For a simple metal, this means the anomaly is expected to be observed below the plasma frequency, moving to higher frequencies for increasing x. In the extreme insulator-rich limit $x\to 1$, Eq. (15a) gives $\epsilon_m(\omega_a)=-\epsilon_i(1-L_m)/L_m$, corresponding to the condition for a singularity in the polarizability[10] of an isolated metallic ellipsoid immersed in a medium of dielectric constant ϵ_i. Naturally in the opposite limit $x\to 0$, Eq. (15b) gives the condition for a singularity in the polarizability of an isolated insulating ellipsoid immersed in a metallic medium. In real metals the presence of a finite $\mathrm{Im}\epsilon_m(\omega)$ damps the anomaly, thereby removing the singularity. The strength of the resulting peak in $\epsilon(\omega)$ is then inversely proportional to $\mathrm{Im}\epsilon_m(\omega)$ and is a function of concentration, decreasing to zero as $x\to 1$ in Eq. (7), and as $x\to 0$ in Eq. (8).

The nature of the anomaly in the continuous-insulator regime has been discussed in detail by Marton and Lemon[19] for the Maxwell-Garnett theory ($L_m=\frac{1}{3}$). It is derived from the usual dc conduction resonance in a metal but is pushed to optical frequencies because of the small particle microstructure. In a rough way, the frequency ω_a represents the boundary between the low-frequency behavior, characteristic of an insulator [Eq. (14a)], and the high-frequency behavior, in which the metallic properties of the metal-insulator composite become apparent. In the continuous-metal regime, the anomaly is actually an additional resonance caused by the insulating inclusions in the metal matrix. This resonance has been treated by Galeener[11] for the case of a small concentration of voids in an amorphous Ge matrix. In principle, measurements of ω_a over the entire range of x can provide another means of optically determining the metallike-to-insulatorlike transition.

In order to observe a strong dielectric anomaly, one should choose metals that have small interband contributions to $\epsilon_m(\omega)$ below the plasma frequency. In that case, there is no chance that the anomaly can be confused with interband absorption processes. Furthermore, the small value of $\mathrm{Im}\epsilon_m^{(i)}(\omega)$ reduces the damping of the anomaly, thereby enhancing its strength. In these respects Ag is an excellent choice for such an investigation, so that a strong anomaly should appear in a frequency range in which no such effects are normally seen. In the case of Au, the onset of strong interband absorption[13] in the visible considerably increases the value of $\mathrm{Re}\,\epsilon_m(\omega)$ and permits Eqs. (15) to be satisfied at frequencies just below the onset of the interband absorption. Thus, in the Au-SiO_2 system the dielectric anomaly should appear as a precursor to the interband absorption peak.

3. *Plasma Resonance*

The Maxwell-Garnett theory predicts a shift of the metal plasma frequency ω_p to lower frequencies as the concentration of insulator is increased. This shift has been discussed in detail by Marton and Lemon[19] for the special case of a free-electron metal $\epsilon_m^{(i)}(\omega)=0$. The shift in ω_p predicted by the theory can be obtained from Eqs. (7) and (8) by setting the real part of $\epsilon(\omega_p)$ equal to zero and solving for the required $\epsilon_m(\omega_p)$. The condition for the plasma frequency can be estimated easily if we again neglect the damping contribution to the metal dielectric constant. We find[20]

$$\epsilon_m(\omega_p)=-\frac{\epsilon_i x(1-L_m)}{1-x(1-L_m)} \quad \text{(continuous insulator)}, \tag{16a}$$

$$\epsilon_m(\omega_p)=0 \quad \text{(continuous metal)}. \tag{16b}$$

Thus, in the continuous-metal regime, where the

metal particles join together to form extended networks, no change in ω_p is expected. As more insulator is added, the particles separate, and the plasma frequency is predicted to occur at frequencies for which ϵ_m is increasingly more negative, e.g., lower frequencies for a simple metal. In the limit $x \to 1$, Eq. (16a) yields $\epsilon_m(\omega_p) = -\epsilon_i(1 - L_m)/L_m$. so that ω_p corresponds to the frequency ω_a given by Eq. (15a) for $x = 1$. Naturally the strength of the plasma resonance, as represented by the energy-loss function $\mathrm{Im}\epsilon^{-1}(\omega_p)$, vanishes in this limit. From these considerations, one sees that the observation of a sudden drop in ω_p would be a signal of the transition from the continuous-metal to the continuous-insulator regime. However, since longitudinal plasmons can not couple to transverse photons, a perpendicular incidence transmission experiment is not capable of detecting plasmons directly.[21] Experiments designed to detect the predicted shift in ω_p are presently underway.

IV. DISCUSSION

We shall first briefly review the experimental results presented in Sec. II. The electron micrographs given in Figs. 1 and 2 for the Au-SiO_2 and Ag-SiO_2 films demonstrate the evolution of the microstructure from a continuous metallic film, through a labyrinth structure, to a system of distinct metal particles separated by SiO_2. The electrical and optical properties are closely correlated with the microstructure. The electrical resistivities, shown in Fig. 3, rise abruptly at the composition which has approximately 40-vol% SiO_2. This abrupt increase is a result of the transition to an isolated particle structure, as indicated in Figs. 1 and 2. For SiO_2 concentrations larger than 50 vol%, the resistivity of the granular metals was observed to increase with decreasing temperature. This behavior is characteristic of electrical conduction due to tunneling between isolated metal particles. The metal activation energy arises from the charging energy required to add an electron to a neutral grain.[9] The optical properties, as determined from the experimental results, Figs. 4 and 8, can be summarized as follows: (i) For compositions less than about 40-vol% SiO_2, the infrared behavior is characterized by an increasing transmission with decreasing wavelength. Above 40-vol% SiO_2 the transmission is observed to decrease slightly with decreasing wavelength. The SiO_2 concentration $x = 0.4$ at which the transition in the infrared behavior is observed coincides with that for which the electrical resistivity increases abruptly (Fig. 3). (ii) An absorption peak in the visible develops with increasing SiO_2 concentration. This peak, characteristic of neither the pure metal nor SiO_2, is related to the microstructure of the granular film. The wavelength λ_A, corresponding to the absorption peak, is plotted as a function of SiO_2 concentration x in Figs. 5 and 9 for the case of Ag and Au, respectively. (iii) A sharp peak in the transmission spectra persists to the highest concentrations of SiO_2. The wavelength λ_T for the occurrence of the peak is plotted against x in Figs. 5 and 9.

A. Optical Properties of Ag-SiO_2

We now compare in detail the experimental results with the theoretical predictions. In Figs. 6 and 7 are shown the calculated transmission spectra for Ag-SiO_2 films, assuming a thickness of 450 Å. The curves in Fig. 6 were calculated using Eq. (8) with a depolarization factor $L_i = 0.9$ for the SiO_2 inclusions in a Ag continuum, while those in Fig. 7 were calculated from Eq. (7) assuming spherical metal particles, $L_m = \frac{1}{3}$ (the Maxwell-Garnett theo-

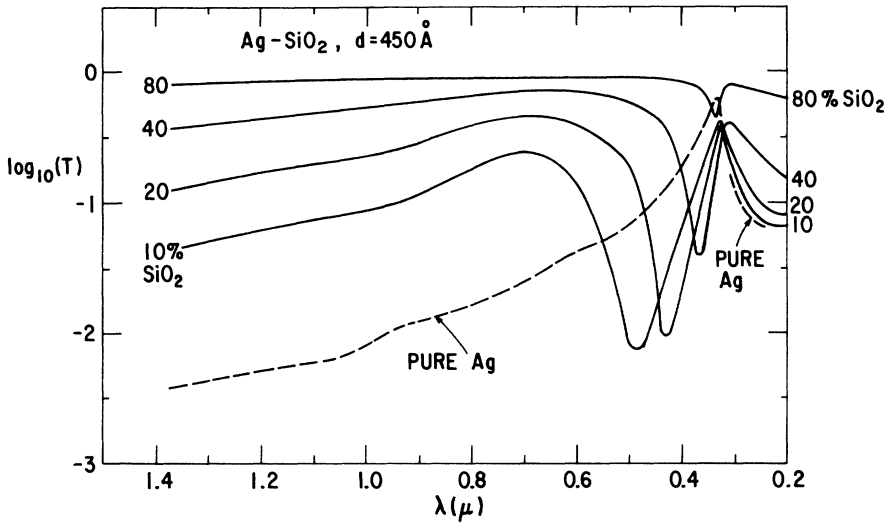

FIG. 6. Computed optical densities for pure silver (dashed curve) and granular Ag-SiO_2 (full curves) as a function of wavelength λ. The volume percents of SiO_2 are indicated. The curves were computed from Eq. (8) assuming inclusions of SiO_2 with depolarization factor $L_i = 0.9$ in an Ag continuum. The dielectric constant for SiO_2, $\epsilon_i = 2.2$, and those for Ag (Ref. 12) were used.

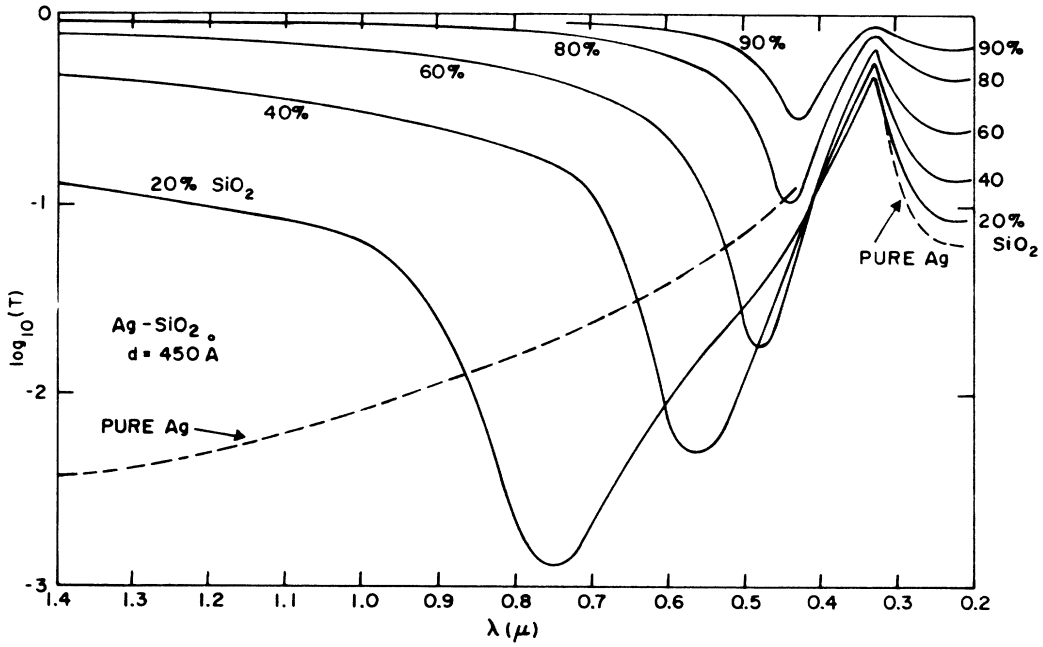

FIG. 7. Computed optical densities for pure silver (dashed curve) and granular Ag-SiO_2 (full curves) as a function of wavelength λ. The volume percents of SiO_2 are indicated. The curves were computed from Eq. (7) assuming silver spheres (depolarization factor $L_m = \frac{1}{3}$) in an SiO_2 continuum. The dielectric constant for SiO_2, $\epsilon = 2.2$, and those for Ag (Ref. 12) were used.

ry), in an SiO_2 continuum. For the dielectric constants of the metal, ϵ_m, we employed published values,[12] modified to include the finite mean free path of the electrons (see Sec. IIID). The constant value[17] $\epsilon_i = 2.2$ was used for the dielectric constant of SiO_2. The spectra for samples in Fig. 4 with $x \geq 0.36$ agree qualitatively with the corresponding calculated curves in Fig. 7 over the entire measured range of wavelengths. Specifically, the infrared behavior is characteristic of that of an insulator, i.e., high transmission which is weakly dependent on wavelength. Furthermore, the position of the absorption peak in the visible is confirmed, although the strength of the peak is somewhat smaller than expected. The experimental data for samples with $x \leq 0.28$ agree with the calculated curves in Fig. 6 in the infrared region (metallike behavior, i.e., increasing transmission with decreasing wavelength), but the absorption peak in the visible disappears at small values of x more rapidly than is predicted by the theory. The spectrum for the film that contains 6-vol% SiO_2 is very close to that calculated for pure Ag (Figs. 6 and 7).

We see that the optical data in the infrared indicate that for $x \lesssim 0.36$ the microstructure consists of a metallic continuum with SiO_2 inclusions, while for $x \gtrsim 0.36$ the microstructure is one of isolated metallic particles in a dielectric medium. Thus, the microstructure, as deduced from the optical data, is in agreement with the observations from electron microscopy (Figs. 1 and 2).

In Fig. 5 are compared the experimental and calculated values of the wavelengths λ_A and λ_T for the absorption peak and the peak in the transmission, respectively. The curves for λ_A for the isolated-metal-particle model were calculated using Eq. (7) with depolarization factors corresponding to spheres ($L_m = \frac{1}{3}$) and cylinders ($L_m = \frac{1}{2}$) with their axes perpendicular to the film. The curve for λ_A for the continuous-metal model was computed from Eq. (8) using the value $L_i = 0.9$, corresponding to platelike inclusions of SiO_2 with the plates perpendicular to the plane of the film. For small values of x, the experimental data for λ_A cross from the curve for SiO_2 plates to that for Ag cylinders. For larger values of x the experimental data generally fall between the curves for Ag cylinders and Ag spheres. Thus, the shapes of the particles deduced from Fig. 5 are qualitatively in agreement with those observed by the electron microscope. The calculated value $\lambda_T = 3200$ Å is independent of x for the case of Ag spheres and for the case of SiO_2 plates for $x \lesssim 0.35$. Indeed this prediction is in agreement with the experimental results shown in Fig. 5.

A significant discrepancy between the experimental results for Ag-SiO_2 (Fig. 4) and the theoretical

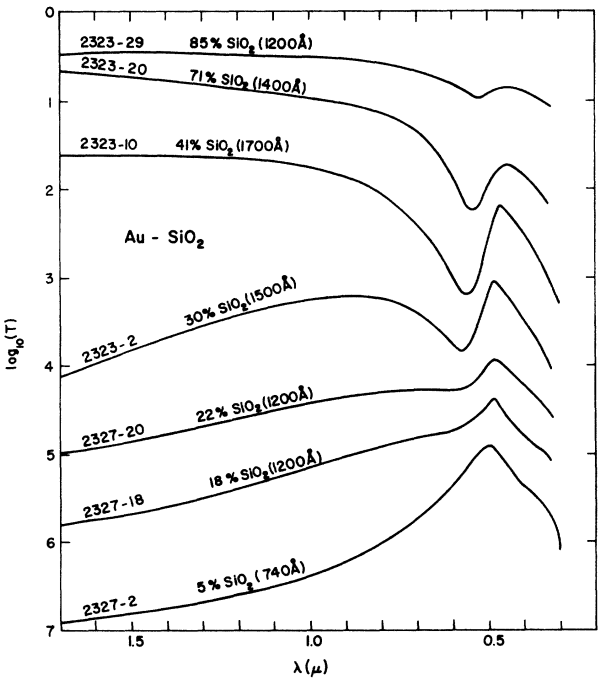

FIG. 8. Logarithms of the optical transmission T of Au-SiO_2 films, measured at room temperature, as a function of wavelength of light. The sample numbers, volume percent SiO_2, and thicknesses are indicated in the figure. The first part of the sample number identifies the particular film strip and target geometry used (see Table I). The second part of the number indicates the distance of the sample (in inches multiplied by 10) measured from the metal-rich end of the strip. For clarity the curves are displaced vertically with respect to one another.

predictions (Figs. 6 and 7) is the observed rapid disappearance of the dielectric anomaly as $x \to 0$, while the calculations predict a more gradual decrease in the magnitude of the absorption peak such that, for values of x as small as 0.1, a substantial peak should still be observed. A possible explanation for this discrepancy involves the breakdown of the assumption that the insulator dielectric constant ϵ_i is pure real. At small values of x, the insulating regions may be sufficiently thin so that electron tunneling through these regions can give rise to an appreciable imaginary contribution to ϵ_i. For example, the value $\mathrm{Im}\epsilon_i = 5$ is sufficient to suppress the absorption peak in Ag-SiO_2 at $x = 0.1$ and reproduce the observed behavior for this composition. This value of $\mathrm{Im}\epsilon_i$ corresponds to an effective tunneling conductance $\sigma_T = 1.7 \times 10^3\ \Omega^{-1}\ \mathrm{cm}^{-1}$. The observed dc conductance for this composition, $\sigma \cong 10^5\ \Omega^{-1}\mathrm{cm}^{-1}$, is still much larger than σ_T, so that tunneling through the insulator does not significantly alter the predominant conduction process (percolation through connected metal networks). If we assume a tunneling barrier of 1 eV, the estimated value of σ_T implies an effective insulator thickness[22] of about 5 Å, somewhat smaller than is observed in the electron microscopy. However, it is plausible that the apparent penetration of very small metal particles into the insulator, as suggested by the electron microscopy, can provide enhanced conduction through considerably thicker insulating regions, thereby leading to the required value of σ_T. We do not believe that the rapid disappearance of the absorption peak can be due to an underestimate of the damping contribution to ϵ_m. To show this we calculate that a value $\mathrm{Im}\epsilon_m \gtrsim 25$ is necessary to suppress the peak at $x = 0.1$ in Ag-SiO_2. Such a large value of $\mathrm{Im}\epsilon_m$ is considered extremely improbable since (a) adjusting τ in Eq. (10) to give the maximum value of the free-electron contribution to $\mathrm{Im}\epsilon_m$ yields only $\mathrm{Im}\epsilon_m^{(f)} = \frac{1}{2}(\tilde{\omega}_p/\omega)^2 = 6.5$ for Ag ($\hbar\tilde{\omega}_p/e = 9.2$ eV[12]) at $\lambda = 0.485\ \mu$, and (b) the interband contribution $\mathrm{Im}\epsilon_m^{(i)}$ is only about[12] 0.2 in this frequency range.

B. Optical Properties of Au-SiO_2

The computed transmission spectra for the Au-SiO_2 films are shown in Figs. 10 and 11. The procedure employed to calculate these curves was the same as for the case of Ag-SiO_2 except that the thickness was taken to be 1300 Å and, of course, the values of the Au dielectric constants[13] were used.

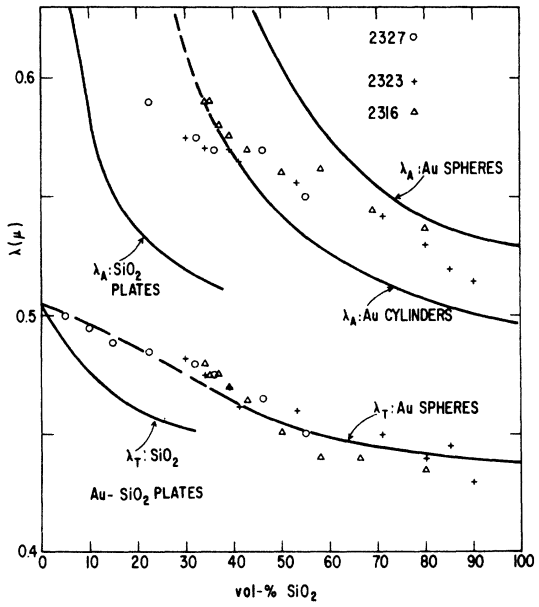

FIG. 9. Absorption-peak wavelength λ_A and the transmission-peak wavelength λ_T as a function of wavelength for several Au-SiO_2 samples. The curves were calculated from Eqs. (7) and (8) for the particle shapes indicated in the figure. The dielectric constants of SiO_2 ($\epsilon_i = 2.2$) and that of Au (Ref. 13) were used.

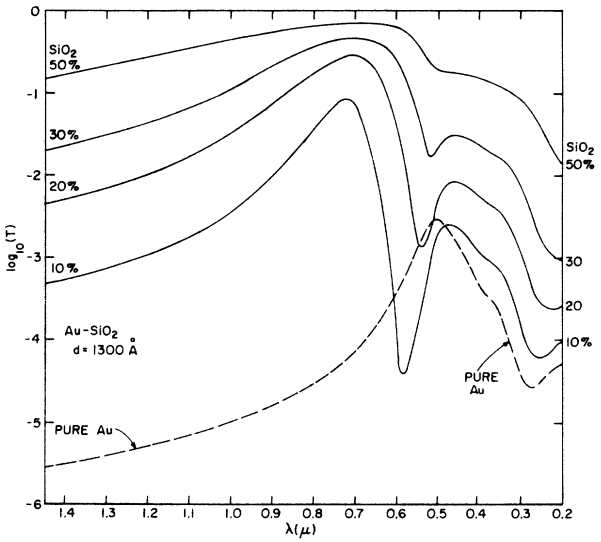

FIG. 10. Computed optical densities for pure gold (dashed curve) and granular Au-SiO_2 (full curves) as a function of wavelength λ. The volume percents of SiO_2 are indicated. The curves were computed from Eq. (8) assuming inclusions of SiO_2 with a depolarization factor $L_i = 0.9$ in an Au continuum. The dielectric constant for SiO_2, $\epsilon_i = 2.2$, and those for Au (Ref. 13) were used.

The optical properties of the Au-SiO_2 films exhibit similar behavior to those of the Ag-SiO_2 films. The major difference between the two systems is that, while in the case of Ag-SiO_2 λ_T was independent of x (see Figs. 4 and 5), for the Au-SiO_2 system λ_T is observed to decrease with x (see Figs. 8 and 9). We note from Fig. 9 that the experimental data for λ_T fall very close to the calculated curve for Au spheres over the entire range of x, even for $x \lesssim 0.4$. This is contrary to our expectation that for $x \lesssim 0.4$, λ_T should decrease more rapidly for small values of x according to the theoretical curve for the model of SiO_2 plates.

V. CONCLUSION

Electron microscopy studies have shown that granular Ag-SiO_2 and Au-SiO_2 exhibit an abrupt matrix inversion in which, at concentrations below approximately 50-vol% SiO_2, the material consists of SiO_2 inclusions in a metallic matrix, while above 50-vol% SiO_2 its microstructure consists of separated metallic particles embeedded in an insulating matrix. This metallike-to-insulatorlike transition manifests itself in the electrical and optical properties of the material. The electrical resistivity is observed to increase rapidly in the concentration region near the transition. At the same time the infrared transmission changes from metallic to dielectric behavior. With the exception of the metal-rich Au-SiO_2 transmission peaks, the positions of the absorption and transmission peaks in the visible are explained in terms of a generalized Maxwell-Garnett theory. This agreement indicates that the size of the metal particles (average particle size as small as 20 Å for 90-vol% SiO_2) does not significantly alter their optical constants, aside from the effect of increased boundary scattering. The theory and experiment disagree in the magnitude of the absorption peaks; the experimental

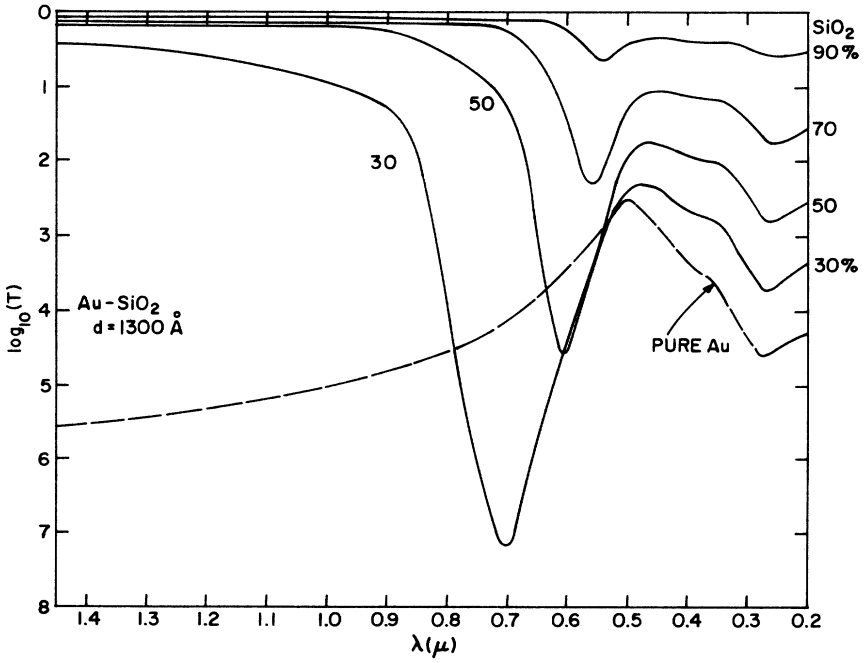

FIG. 11. Computed optical densities for pure gold (dashed curve) and granular Au-SiO_2 (full curves) as a function of wavelength λ. The volume percents of SiO_2 are indicated. The curves were computed from Eq. (7) assuming gold spheres (depolarization factor $L_m = \frac{1}{3}$) in an SiO_2 continuum. The dielectric constant for SiO_2, $\epsilon = 2.2$, and those for Au (Ref. 13) were used.

value is higher and drops off more rapidly with decreasing SiO_2 concentration than predicted theoretically. This discrepancy may arise from the uncertainty in the composition for metal-rich samples and from an imaginary component of the dielectric constant of SiO_2.

The observed abrupt matrix inversion effect and the attendant sharp rise in the resistivity appears to be characteristic of granular Ag-SiO_2 and Au-SiO_2. In contrast with these materials, Ni-SiO_2,[23] Al-SiO_2,[24] and Al-Al_2O_3[25] do not exhibit the labyrinth pattern, and the rise in resistivity near the metal-to-nonmetal transition is more gradual.[24,26]

The applicability of the Maxwell-Garnett theory to granular metal systems over an extended range of metal-particle concentrations has been convincingly demonstrated. The effect of particle shapes has been included in the theory in a simple and consistent manner. The results of the analysis of the experimental transmission spectra of the Ag-SiO_2 and Au-SiO_2 films agree with the electron microscopy in that (i) in the continuous-insulator regime, the metal particles in the sputtered films are cylindrical with their axes normal to the plane of the film, and (ii) in the continuous-metal regime, the SiO_2 inclusions are platelike with a large ($L_i \cong 0.9$) effective depolarization factor. The ability of optical measurements to determine such details of the microstructure of granular metals is remarkable in view of the fact that the wavelength of light is so much larger than the scale of the microstructure. The successful experimental discernment of these details illustrates the power of the simple Maxwell-Garnett theory.

ACKNOWLEDGMENTS

We thank J. J. Hanak for the use of his computer programs for determining the compositions of the granular metals and Y. Arie for his technical assistance in the preparation of the films. We are also grateful to J. I. Gittleman for valuable discussions and suggestions.

[1] W. Hampe, Z. Phys. **152**, 470 (1958); Z. Phys. **152**, 476 (1958).

[2] G. Rasigni and P. Rouard, J. Opt. Soc. Am. **53**, 604 (1963); S. Yoshida, T. Yamaguchi, and A. Kinbara, J. Opt. Soc. Am. **61**, 62 (1971); J. Opt. Soc. Am. **61**, 463 (1971); J. Opt. Soc. Am. **62**, 634 (1972); J. Opt. Soc. Am. **62**, 1415 (1972).

[3] R. H. Doremus, J. Chem. Phys. **40**, 2389 (1964).

[4] R. H. Doremus, J. Appl. Phys. **37**, 2775 (1966).

[5] R. H. Doremus, J. Chem. Phys. **42**, 414 (1965).

[6] N. C. Miller, B. Hardiman, G. A. Shirn, J. Appl. Phys. **41**, 1850 (1970).

[7] J. C. Maxwell-Garnett, Philos. Trans. R. Soc. Lond. **203**, 385 (1904); Philos. Trans. R. Soc. Lond. **205**, 237 (1906).

[8] J. J. Hanak, H. W. Lehman, and R. K. Wehner, J. Appl. Phys. **43**, 1666 (1972).

[9] C. A. Neugebauer and M. B. Webb, J. Appl. Phys. **33**, 74 (1962); P. Sheng and B. Abeles, Phys. Rev. Lett. **28**, 34 (1972); Phys. Rev. Lett. 31, 44 (1973).

[10] See, for example, L. D. Landau and E. M. Lifshitz, *Electrodynamics of Continuous Media* (Addison-Wesley, Reading, Mass., 1960), pp. 20–27, 42–45.

[11] F. L. Galeener, Phys. Rev. **27**, 421 (1971); Phys. Rev. **27**, 1716 (1971).

[12] H. Ehrenreich and H. R. Philipp, Phys. Rev. **128**, 1622 (1962).

[13] B. R. Copper, H. Ehrenreich, and H. R. Philipp, Phys. Rev. **138**, A494 (1965).

[14] A more sophisticated theory of electron scattering small metal particles was developed by A. Kawabata and R. Kubo, J. Phys. Soc. Jap. **21**, 1772 (1966).

[15] W. J. Doyle, Phys. Rev. **111**, 1067 (1958).

[16] J. P. Marton and M. Schlesinger, J. Appl. Phys. **40**, 4529 (1969).

[17] *A. I. P. Handbook* (McGraw-Hill, New York, 1972), p. 6-28.

[18] The supplementary conditions $|\epsilon_m(\omega)| \gg (1 - L_m)\epsilon_i/L_m$ and $|\epsilon_m(\omega)| \gg L_i\epsilon_i/(1 - L_i)$ must be satisfied in the continuous-insulator and continuous-metal regimes, respectively.

[19] J. P. Marton and J. R. Lemon, Phys. Rev. B **4**, 271 (1971).

[20] For $x > 0$, Eq. (8) has a second solution for $\epsilon = 0$ which will give rise to a subsidiary resonance at a frequency below both the main plasma resonance and the frequency ω_a for the dielectric anomaly.

[21] Sometimes, one can deduce the value of ω_p from the position of the strong transmission peak. Such is the case for Ag, which has a well-defined transmission peak near the plasma frequency $\hbar\omega_p/e \simeq 3.8$ eV. However, such a peak is not a definitive determination of ω_p; it is more nearly associated with the frequency for which $\mathrm{Re}\epsilon_m(\omega) = 1$, the best dielectric match to vacuum. Indeed, while ω_p is predicted to shift in granular Ag-SiO_2 approximately according to Eq. (16a), the position of the peak in the transmission should remain essentially unchanged (see Fig. 7).

[22] The value $d_T \simeq 5$ Å for the insulator thickness was estimated from the formula $\sigma_T = \tilde{\omega}_p^2\tau_T/4\pi$, where τ_T is the relaxation time for tunneling. To calculate τ_T, we used the expression $\tau_T = d\,t/v_F$ [B. Abeles, R. W. Cohen, and W. R. Stowell, Phys. Rev. Lett. **18**, 902 (1967)], where d is an effective metal-particle size, t is the tunneling transmission coefficient, and v_F is the Fermi velocity. The WKB formula for rectangular tunneling barriers was employed: $t = \exp[-2(2m^*V_0/\hbar^2)^{(1/2)}d_T]$, where m^* is the effective mass of the tunneling electrons and V_0 is the effective tunneling-barrier height. Taking $\sigma_T = 1.7 \times 10^3\ \Omega$ cm, $\hbar\tilde{\omega}_p/e = 9.2$ eV (Ref. 12), $d = 100$ Å, $v_F = 10^8$ cm/sec, $m^* = 1$ electron mass, and $eV_0 = 1$ eV, we obtain $d_T \simeq 5$ Å.

[23] M. S. Abrahams, C. j. Buiocchi, M. Rayl, and P. J. Wojtowicz, J. Appl. Phys. **43**, 2537 (1972).

[24] B. Abeles and J. J. Hanak, Phys. Lett. A **34**, 165 (1971).

[25] B. Abeles, R. W. Cohen, and G. W. Cullen, Phys. Rev. Lett. **17**, 632 (1966).

[26] B. Abeles and Ping Sheng, in *Proceedings of the Thirteenth Low-Temperature Physics Conference, Boulder, Colorado, 1972,* edited by R. H. Kropschot and K. D. Timmerhaus (University of Colorado Press, Boulder, Colo., 1973).

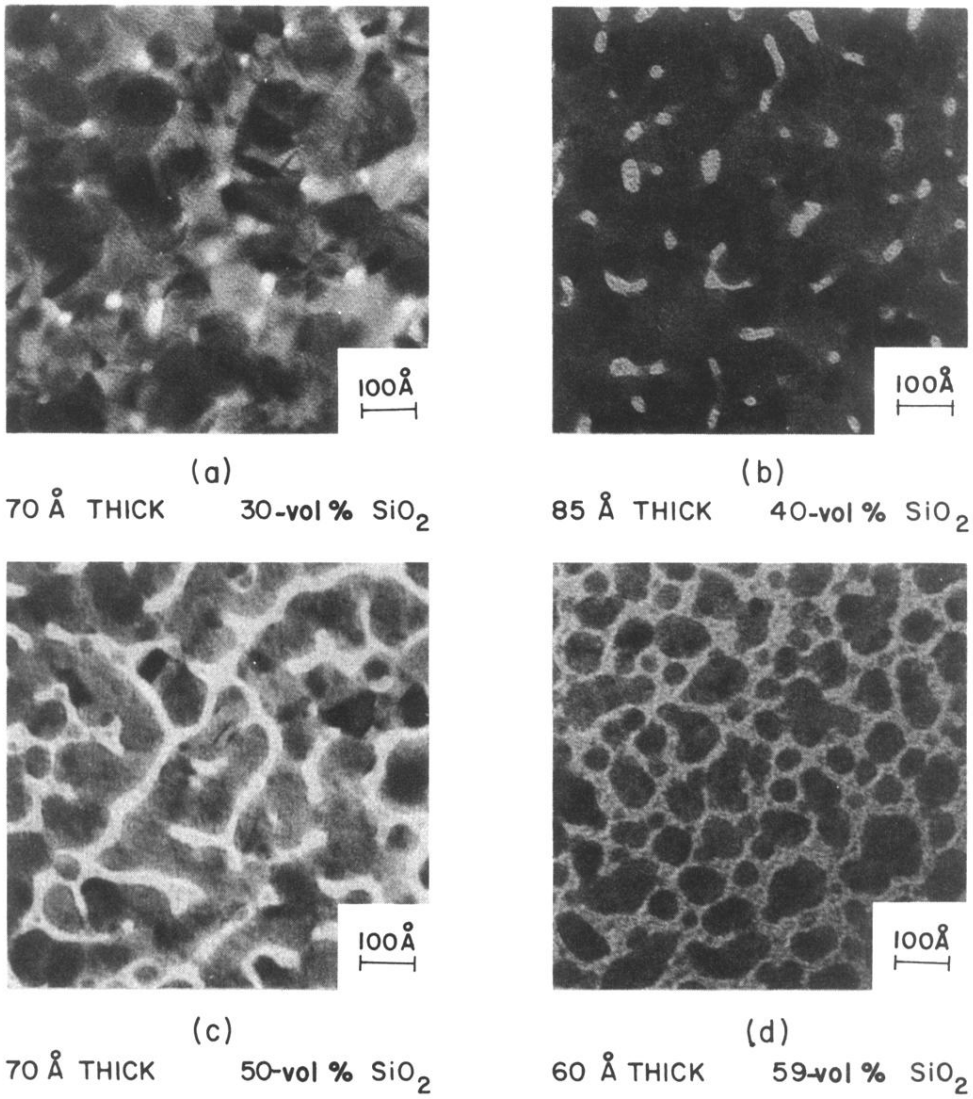

FIG. 1. Electron micrographs of Au-SiO_2 films. Thickness and composition are given in the figure. (a) Au matrix with white circular disks, about 20 Å in diameter, which are probably SiO_2 columns. (b) Au matrix with SiO_2 as thin curved platelets. (c) Au matrix with SiO_2 isolated dendrites. (d) Complete matrix inversion: SiO_2 continuum with isolated Au particles.

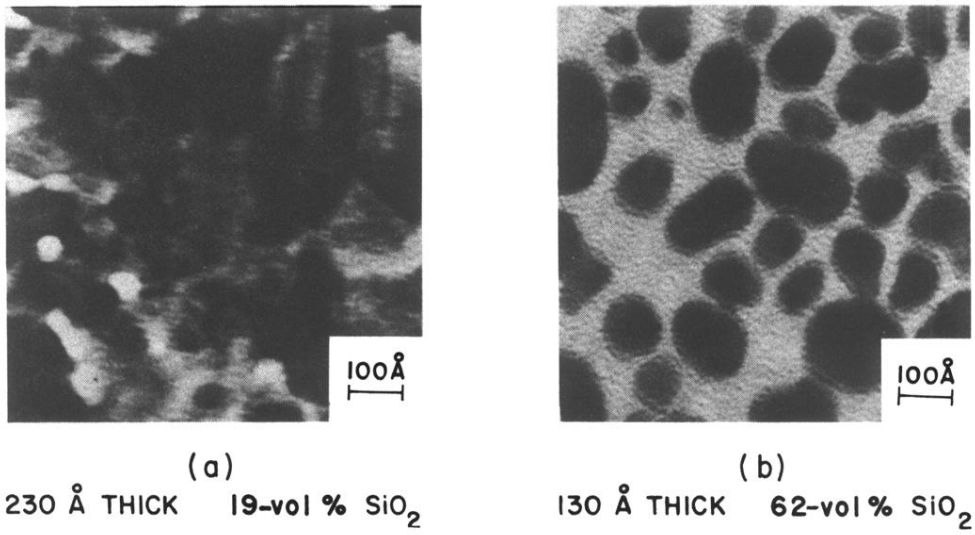

FIG. 2. Electron micrographs of Ag-SiO_2 films. Thickness and composition are indicated in the figure. (a) Ag matrix with white disks which are probably SiO_2 columns. (b) SiO_2 matrix with embedded isolated Ag particles.